New implementation of a non-associated flow rule in rate-independent plasticity

F. Moayyedian[a,*] and M. Kadkhodayan[b]

[a]Department of Mechanical Engineering, Eqbal Lahoori Institute of Higher Education (ELIHE), Mashhad, Khorasan Razavi, P.O. Box 91771-13113, Iran
[b]Department of Mechanical Engineering, Ferdowsi University of Mashhad, Mashhad, Khorasan Razavi, P.O. Box 91775-1111, Iran

Abstract

One of the new research fields in plasticity is related to choosing a proper non-associated flow rule (NAFR), instead of the associated one (AFR), to predict the experimental results more accurately. The idea of the current research is derived from combining von Mises and Tresca criteria in the places of yield and plastic potential surfaces in rate-independent plasticity. This idea is implemented using backward Euler method in non-linear finite element simulation. The results are compared with the experimental data for an internally pressurized thick-walled cylinder and it is demonstrates that, using the proposed NAFR in rate-independent plasticity, the experimental results could be predicted more accurately. Finally, it can be said that the current research confirms the results of the previous works on rate-dependent plasticity (viscoplasticity) in steady state conditions.

1. Introduction

In recent years, employing non-associated flow rule (NAFR) in plasticity for describing the behavior of materials has become very common. Below, the works of other authors on non-linear finite element simulations and also employment of non-associated flow rule are reviewed.

Stoughton and Yoon [1] proposed a non-associated flow rule based on a pressure sensitive yield criterion with isotropic hardening. Significance of their work was in that thee model distorted the shape of the yield

function in tension and compression and fully accounted for the strength differential effect (SDE). Oliver et al. [2] presented an implicit/explicit scheme for non-linear constitutive models. Their proposed scheme provided additional computability to the solid mechanic problems, in which robustness was an important issue. This scheme could provide important advantageous in terms of computational cost compared to the implicit integration schemes. Stoughton and Yoon [3] showed that, under certain conditions, an intermediate solution existed to the equations of motion for the dynamic elastic-plastic

*Corresponding author
Email address: farzad.moayyedian@gmail.com

deformation of materials using constitutive laws based on non-associated flow rule. They suggested that an initial perturbation in the stress could develop from a quiescent state on the yield surface. The existence of this indeterminate solution was alleged to theoretically discourage the use of non-associated flow rules for both dynamic and quasi-static analyses. Cvitanic et al. [4] developed a finite element formulation based on non-associated plasticity. The yield and plastic potential were considered as two different functions with a functional form. Algorithmic formulations of constitutive models that utilized associated or non-associated flow rule were derived by the application of implicit return mapping procedure. Valoroso and Rosati [5] presented a general projected algorithm for general isotropic three-invariant plasticity method under plane stress conditions. They provided a closed-form intrinsic algorithm linearization and a novel expression of the consistent tangent tensor. Stoughton and Yoon [6] calibrated and evaluated five material models ranging in complexity from a von Mises model based on isotopic hardening to a non-associated flow rule model based on anisotropic hardening. The model was expected to lead to significant improvement in stress prediction under the conditions dominated by proportional loading. It was expected to directly improve the accuracy of spring back, tearing, and earning predictions for these processes. Gao et al. [7] used experimental and numerical studies and demonstrated that stress state had strong effects on both plastic response and ductile fracture behavior of an aluminum 5083 alloy. As a result, the hydrostatic stress and the third invariant of the stress deviator (related to the Lode angle) needed to be incorporated into the material modeling. Taherizadeh et al. [8] developed an anisotropic material model based on a non-associated flow rule, mixed isotropic-kinematic hardening and implemented it in a user-defined material (UMAT) subroutine for the commercial finite element code ABAQUS. Their results showed that their non-associated, mixed hardening model significantly improved the prediction of earing in the cup drawing process and the prediction of springback in the

sidewall of drawn channel sections, even when a simple quadratic constitutive model was used. Taherizadeh et al. [9] developed a generalized finite element formulation of stress integration method for non-quadratic yield functions and potentials with mixed non-linear hardening under non-associated flow rule. Different approaches to analyzing the anisotropic behavior of sheet materials were also compared. Gao et al. [10] described a plasticity model for isotropic materials, which was a function of the hydrostatic stress as well as the second and third invariants of the stress deviator with special attention to adopting the non-associated flow rule and presenting its finite element implementation, including integration of the constitutive equations using backward Euler method and formulation of the consistent tangent moduli. Moayyedian and Kadkhodayan [11] presented a new first and second differentiation of a general yield surface and implemented it for different time stepping schemes including explicit, trapezoidal implicit, and fully implicit time stepping schemes in rate-dependant plasticity. Moayyedian and Kadkhodayan [12] presented a new non-associated viscoplastic flow rule (NAVFR) by combining von Mises and Tresca loci in the place of yield and plastic potential functions and vice versa using fully implicit time stepping scheme. Moayyedian and Kadkhodayan [13] used the new first and second differentiation of a yield function and comparing explicit, semi-implicit and implicit algorithms in rate-independent plasticity and showed that the fully implicit scheme was more accurate than others considering the experimental results. Moayyedian and Kadkhodayan [14] introduced a Modified Yld2000-2d II by inserting modified Yld2000-2d and Yld2000-2d in place of yield and plastic potential functions, respectively, to depict the behavior of anisotropic pressure sensitive sheet metals. Moayyedian and Kadkhodayan [15] modified the Burzynski criterion used for pressure-sensitive isotropic materials for anisotropic pressure sensitive sheet metals based on non-AFR to describe the behavior of asymmetric anisotropic sheet metals. Ghaei and Taherizadeh [16] presented a model to describe the anisotropic behavior of

sheet metals at both yield stresses and plastic strain ratios using the non-AFR and quadratic yield and potential functions. Additionally, to reproduce accurate prediction of cyclic plastic deformation phenomena, a two-surface mixed isotropic-nonlinear kinematic hardening model was combined with the quadratic non-AFR anisotropic formulation.

The main goal of this study is derived from combining von Mises and Tresca surfaces in place of yield and plastic potential surfaces. Although von Mises and Tresca surfaces are independent from hydrostatic pressure, it is demonstrated that the proposed NAFR can predict the experimental results more accurately than the AFR. To show the ability of the new proposed method, an internally pressurized thick-walled cylinder is considered with perfectly plastic and linear-isotropic hardening behaviors of material and coded in Compaq Visual Fortran Professional, Edition 6.5.0, and the obtained results are compared with the experimental data. To model this problem, the following references in plasticity and non-linear finite element are employed: Owen and Hinton [17], Souza Neto et al. [18], Simo and Hughes [19], Zienkiewicz and Taylor [20], Crisfield [21], Hill [22], and Khan and Hung [23]. It is shown that, with increasing hardening and also approaching of the Lode parameter to ± 1, $(\Gamma \rightarrow \pm 1)$, the difference between the presented NAFR and the corresponding AFR increases.

In the current research, the computation of the first and second differentiations of a yield and plastic potential function in its simplified matrix form is based the earlier works by Moayyedian and Kadkhodayan [11-13]. Finally, it can be said that the proposed NAFR can be implemented in both rate- and rate-independent plasticity using the proposed procedure.

2. Matrix formulation of backward Euler scheme with NAFR

To model a thick walled pressure vessel it is demonstrated the Backward Euler method is more accurate than the others by Moayyedian

and Kadkhodayan [13] therefore this method is accepted in current research. For three dimensional stress space any 6×1 vector is shown with symbol $\{\ \}$ and any 6×6 matrix is shown with symbol $[\ ]$. In the following the formulation of backward Euler method with non-associated plasticity in non-linear finite element is derived.

The yield condition in a state of stress can be shown with following equation:

$$\begin{cases} F(\sigma, \kappa) = f(\sigma) - \sigma_Y(\kappa) = 0 \\ G = g(\sigma) \end{cases} \tag{1}$$

in which F is yield condition and f defines yield surface. $G = g$ defines the plastic potential surface, $\{\sigma\}$ is the stress vector, and κ is the hardening parameter. It is assumed that $d\kappa = \{\sigma\}^T \{d\varepsilon_p\}$; therefore, the work hardening hypothesis is confirmed. The increment direction of the plastic strain vector $\{\ \}$ from NAFR can be found as follows:

$$\{d\varepsilon_p\} = d\lambda \{b\} \tag{2}$$

where $d\lambda$ is the plastic multiplier and $\{b\}$ is:

$$\{b\}^T = \left\{\frac{\partial g}{\partial \sigma}\right\}^T =$$

$$\left\{\frac{\partial g}{\partial \sigma_x}, \frac{\partial g}{\partial \sigma_y}, \frac{\partial g}{\partial \sigma_x}, \frac{\partial g}{\partial \tau_{yz}}, \frac{\partial g}{\partial \tau_{xz}}, \frac{\partial g}{\partial \tau_{xy}}\right\} \tag{3}$$

For one-dimensional linear-isotropic hardening with NAFR in any load step, it can be shown that:

$$\sigma_{n+1} = \sigma_Y + H'\left(\bar{\varepsilon}_{p_n} + \Delta\bar{\varepsilon}_{p_{n+1}}\right) =$$

$$\sigma_Y + H'\left(\bar{\varepsilon}_{p_n} + \frac{g_{n+1}}{f_{n+1}} \Delta\lambda_{p_{n+1}}\right) \tag{4}$$

where H' is the plastic modulus and $\bar{\varepsilon}_p$ is the effective plastic strain. Then, the equations in Eq. (5) can be obtained. The following steps

have to be followed in a fully implicit algorithm:

$$
\begin{cases}
F_{n+1} = F\left(\sigma_{n+1}, \dfrac{g_{n+1}}{f_{n+1}}\Delta\lambda_{n+1}\right) = \\[2mm]
f(\sigma_{n+1}) - \kappa\left(\dfrac{g_{n+1}}{f_{n+1}}\Delta\lambda_{n+1}\right) = \\[2mm]
f(\sigma_{n+1}) - \left[\sigma_Y + H'\left(\overline{\varepsilon}_{p_n} + \dfrac{g_{n+1}}{f_{n+1}}\Delta\lambda_{n+1}\right)\right] = 0 \\[2mm]
G_{n+1} = g(\sigma_{n+1})
\end{cases}
\tag{5}
$$

1. Assume that plastic loading, i.e. $F_{n+1}^{critical} > 0$, the plastic flow residual $\{R_{n+1}\}$, and the yield condition can be defined as:

$$
\begin{cases}
\{R_{n+1}\} = -\{\varepsilon_{n+1}^p\} + \{\varepsilon_n^p\} + \Delta\lambda_{n+1}\left\{\dfrac{\partial g_{n+1}}{\partial\sigma}\right\} \\[3mm]
F_{n+1} = F\left(\sigma_{n+1}, \dfrac{g_{n+1}}{f_{n+1}}\Delta\lambda_{n+1}\right)
\end{cases}
\tag{6}
$$

where $\{\sigma_{n+1}\} = [D]\left(\{\varepsilon_{n+1}\} - \{\varepsilon_{n+1}^p\}\right)$, in which $\{\varepsilon\}$ is the strain vector and $[D]$ is the elastic stiffness matrix.

2. Linearize the above equation. Because $\{\varepsilon_{n+1}\}$ and $\overline{\varepsilon}_{p_n}$ are assumed to be fixed during return-mapping stage, then $\{\Delta\varepsilon_{n+1}^p\}^{(k)} = -[D]^{-1}\{\Delta\sigma_{n+1}\}^{(k)}$ and we have:

$$
\begin{cases}
\{R_{n+1}\}^{(\kappa)} + [\Xi_{n+1}]^{-1(\kappa)}\{\Delta\sigma_{n+1}\}^{(\kappa)} + \\[2mm]
\{b_{n+1}\}^{(\kappa)}\Delta^2\lambda_{n+1}^{(\kappa)} = 0 \\[2mm]
F_{n+1}^{(\kappa)} + \{a_{n+1}\}^{T(\kappa)}\{\Delta\sigma_{n+1}\}^{(\kappa)} + \\[2mm]
H'\dfrac{g_{n+1}}{f_{n+1}}\Delta^2\lambda_{n+1}^{(\kappa)} = 0
\end{cases}
\tag{7}
$$

Some relations appear in Eq. (8) and the Hessian matrix is in Eq. (9).

3. Solve the linearized problem to obtain Eq. (10).

$$
\begin{cases}
\{a_{n+1}\} = \left\{\dfrac{\partial F_{n+1}}{\partial\sigma}\right\} = \left\{\dfrac{\partial f_{n+1}}{\partial\sigma}\right\} + \\[3mm]
\dfrac{H'\Delta\lambda_{n+1}}{f_{n+1}}\left(\left\{\dfrac{\partial g_{n+1}}{\partial\sigma}\right\} - \dfrac{g_{n+1}}{f_{n+1}}\left\{\dfrac{\partial f_{n+1}}{\partial\sigma}\right\}\right) \\[3mm]
\{b_{n+1}\} = \left\{\dfrac{\partial G_{n+1}}{\partial\sigma}\right\} = \left\{\dfrac{\partial g_{n+1}}{\partial\sigma}\right\}
\end{cases}
\tag{8}
$$

$$
[\Xi_{n+1}] = \left([D]^{-1} + \Delta\lambda_{n+1}\left[\dfrac{\partial b_{n+1}}{\partial\sigma}\right]\right)^{-1}
\tag{9}
$$

$$
\begin{cases}
\Delta^2\lambda_{n+1}^{(k)} = \dfrac{F_{n+1}^{(k)}}{\{a_{n+1}\}^{T(k)}[\Xi_{n+1}]^{(k)}[b_{n+1}]^{(k)} - \dfrac{g_{n+1}^{(k)}}{f_{n+1}^{(k)}}H'} \\[5mm]
\quad - \dfrac{\{a_{n+1}\}^{T(k)}[\Xi_{n+1}]^{(k)}\{R_{n+1}\}^{(k)}}{\{a_{n+1}\}^{T(k)}[\Xi_{n+1}]^{(k)}[b_{n+1}]^{(k)} - \dfrac{g_{n+1}^{(k)}}{f_{n+1}^{(k)}}H'} \\[5mm]
\{\Delta\sigma_{n+1}^{(k)}\} = -[\Xi_{n+1}]^{(k)} \\[2mm]
\left[\{R_{n+1}\}^{(k)} + \{b_{n+1}\}^{(k)}\Delta^2\lambda_{n+1}^{(k)}\right] \\[2mm]
\{\Delta\varepsilon_{n+1}^{p(k)}\} = -[D]^{-1}\{\Delta\sigma_{n+1}^{(k)}\}
\end{cases}
\tag{10}
$$

4. Update the plastic strain $\{\varepsilon_{n+1}^p\}^{(k)}$ and the consistency parameter $\Delta\lambda_{n+1}^{(k)}$ as in Eq. (11) and Eq. (12).

$$
\{\varepsilon_{n+1}^p\}^{(k+1)} = \{\varepsilon_{n+1}^p\}^{(k)} + \{\Delta\varepsilon_{n+1}^p\}^{(k)}
\tag{11}
$$

and

$$
\Delta\lambda_{n+1}^{(k+1)} = \Delta\lambda_{n+1}^{(k)} + \Delta^2\lambda_{n+1}^{(k)}
\tag{12}
$$

The procedure summarized above is simply a systematic application of Newton's method to solve the system of Eq. (6) that results in the computation of the closest point projection from the trial state onto the yield surface. The geometric interpretation of the iteration scheme is illustrated in Fig. 1. Note that, in this implicit procedure, normality is enforced at the final (unknown) iteration. The described procedure

considers non-associated flow rule; if it is assumed that $g = f$, the relations can be obtained for the associated flow rule as well. It is noted that, in the above procedure, convergence is achieved when $\sqrt{\{R_{n+1}\}^T \{R_{n+1}\}}$ and F_{n+1} in Eq. (6) reach the prescribed tolerances.

3. Matrix formulation of consistent elastic-plastic modulus with NAFR

Differentiating the elastic stress-strain relationships and the discrete flow rule gives:

$$\begin{cases} \{d\sigma_{n+1}\} = [D]\big(\{d\varepsilon_{n+1}\} - \{d\varepsilon_{n+1}^p\}\big) \\ \{d\varepsilon_{n+1}^p\} = \Delta\lambda_{n+1}\left[\dfrac{\partial b_{n+1}}{\partial\sigma}\right]\{d\sigma_{n+1}\} \\ + d\Delta\lambda_{n+1}\{b_{n+1}\} \end{cases} \quad (13)$$

Thus, one obtains the following algorithmic relationship:

$$\{d\sigma_{n+1}\} = [\Xi_{n+1}]\big(\{d\varepsilon_{n+1}\} - d\Delta\lambda_{n+1}\{b_{n+1}\}\big) \quad (14)$$

On the other hand, differentiating the discrete consistency condition yields:
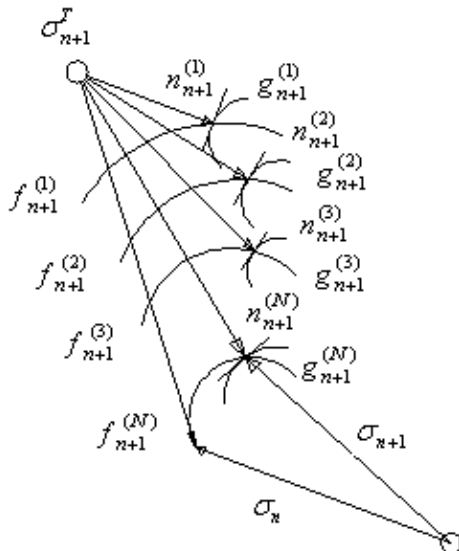
Fig. 1. Iterative procedure of Euler backward under non-associated flow rule, f, yield surface, g, potential surface, n, normal to the potential surface.

$$\{a_{n+1}\}^T \{d\sigma_{n+1}\} - H'\frac{g_{n+1}}{f_{n+1}} d\Delta\lambda_{n+1} = 0 \quad (15)$$

Thus, from Eqs. (14) and (15) we have:

$$d\Delta\lambda_{n+1} = \frac{\{e_D\}^T \{d\varepsilon_{n+1}\}}{\dfrac{g_{n+1}}{f_{n+1}}H' + \{e_D\}^T \{b_{n+1}\}} \quad (16)$$

where,

$$\{e_D\} = [\Xi_{n+1}]\{a_{n+1}\} \quad (17)$$

Finally, substituting Eq. (18) in (14) yields the expression for elastic-plastic relation:

$$\{d\sigma_{n+1}\} = [D_{ep}]_{n+1}\{d\varepsilon_{n+1}\} \quad (18)$$

where the consistent elastic-plastic modulus is defined as follows:

$$[D_{ep}]_{n+1} = [\Xi_{n+1}] - \frac{\{e_D'\}\{e_D\}^T}{\dfrac{g_{n+1}}{f_{n+1}}H' + \{e_D\}^T \{b_{n+1}\}} \quad (19)$$

where,

$$\{e_D'\} = [\Xi_{n+1}]\{b_{n+1}\} \quad (20)$$

It is noted that employing the non-associated flow rule leads the consistent elastic-plastic modulus to become non-symmetric.

The flowchart of non-linear finite element employed in the current research in Fig. 1 is similar to the work done by Moayyedian and Kadkhodayan [12]; but, to use $[D_{ep}]$, the procedure explained in Sections 2 and 3 must be employed.

4. Results and discussion

In this section, an internally pressurized elastic-plastic thick-walled cylinder (as illustrated in Fig. 2) is investigated. The mechanical properties are as follows: Young's modulus of elasticity $E = 2.1 \times 10^4 \dfrac{dN}{mm^2}$, Poisson' ratio

$v = 0.3$, yield stress $\sigma_Y = 24.0 \dfrac{dN}{mm^2}$, plastic modulus $H' = \dfrac{E}{10}$, and the inner and outer radii of the cylinder as $a = 100mm$ and $b = 200mm$, respectively. More explanations of this problem exist in the works done by Moayyedian and Kadkhodayan [11- 13] and Owen and Hinton [17].

Using the relations obtained in the previous sections for NAFR, different yielding criteria and plastic potentials are employed to compare the effects on the obtained results (Fig. 3). In this part, (V) and (T) stand for the von Mises and Tresca criteria, respectively.
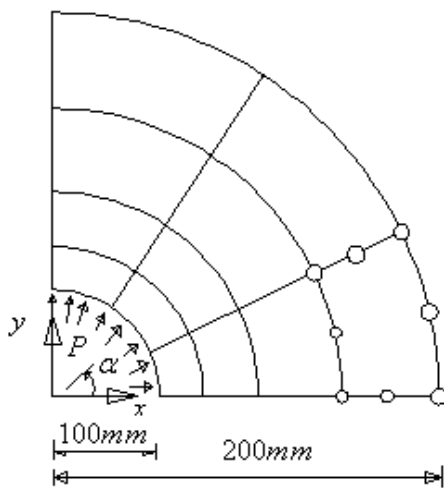
Fig. 2. Mesh employed in the elastic-plastic analysis of an internally pressurized thick cylinder under plane strain conditions.

Moreover, in the forming of $(\square - \square)$, the first and second letters show the yielding criteria and plastic potential used in the analysis, respectively. The results demonstrate that employing von Mises criterion $(V - V)$ overestimates the experimental results as in Marcal [24]; but, using NAFR $(V - T)$ can predict a better estimation than $(V - V)$. Moreover, using Tresca criterion $(T - T)$ underestimates the experimental results and here also using NAFR $(T - V)$ gives better

results than $(T - T)$. It is also observed that, for $\dfrac{b}{a} \leq 2$, using $(T - V)$ and, for $\dfrac{b}{a} \geq 2$, using $(V - T)$ provide better results.

Figs. 4-7 demonstrate the circumferential strain of the outer surface at $\dfrac{r}{a} = 2.4$ with increasing pressure and circumferential stress distributions in the range of $1 \leq \dfrac{r}{a} \leq 2.4$ for perfect-plastic and hardeninig materilas. The results represent that, with increasing the load and hardening, the difference between the presented AFR and NAFR is increased. On the other hand, for the
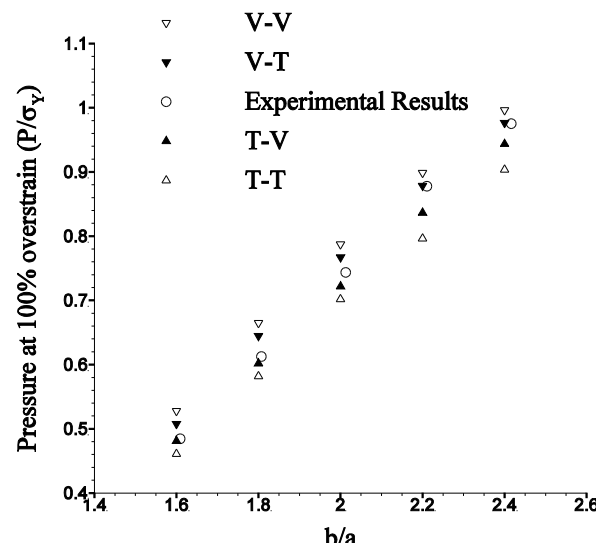
Fig. 3. A Comparing the experimental results and $(V - V)$, $(V - T)$, $(T - V)$, $(T - T)$.

cylinder geometry of $\dfrac{b}{a} = 1.6$, the flow rule of $(T - V)$ gives more accurate results (see Figs. 8-11). These figures show again that, with increasing the load and hardening, the difference between AFR and NAFR is increased.

Now, two important questions emerge, i.e. What is the main reason for the difference between employing AFR and NAFR? and On what conditions does this difference increase?. These questions are discussed below in more detail. The previous results in Figs. 4-11 show that, with increasing the load and hardening, the

difference between AFR and NAFR is increased. Another main reason for this difference can be attributed to the combination of loading (tention-shear). To investigate this issue, the Lode parameter, Γ, is considered $\Gamma = -\sqrt{3}\tan\theta$, where θ is the angle of loading vector in deviatoric plane (Moayyedian and Kadkhodayan [12]). Figures 12-17 show the variation of Lode parameter (in outer surface) with internal pressure, radius (in $\alpha = 0°$), and angle α when AFR based on both von Mises and Tresca yielding criteria is used, respectively. As can be apparent, at pure shear, the orthogonal vectors to Tresca and von Mises surfaces have the same directions (not the same values). Now, when loading is such that $\Gamma \rightarrow 0$, then the difference between the directions of the vectors of plastic strain increment for von Mises and Tresca decreases. On the other hand, when the loading is such that $\Gamma \rightarrow \pm1$, then the difference increases. In other words, as the loading condition varies in such a way that $\Gamma \rightarrow \pm1$, then the difference between AFR and NAFR becomes higher. Figures 13-16 show that the maximum difference between the AFR and NAFR happens in the outer surface of the cylinder. Figures 12-17 demonstrate that, for the current loading condition, the Lode parameter is $\Gamma \cong -0.4$ in the outer surface. The differences between the results obtained by considering perfect-plastic behavior of matrials in Figs. 4 and 8 and also Figs. 5 and 9 are solely because of the combination of loading. However, these differences become higher when, in addition to the combination of loading, the isotropic hardening is also considered (see Figs. 6 and 10 and also Figs. 7 and 11). Therefore, for the problems with non-linear isotropic hardening in conjunction with the load condition in deviatoric plane as $\Gamma \rightarrow \pm1$, the difference between the presented NAFR and the corossponding AFR would be maximum. Figure 18 shows the variation of Lode parameter with different ratios of $\dfrac{b}{a}$. It is evident that, for both $(V - V)$ and $(T - T)$ associated flow rules, there is almost no change for Lode parameter versus ratio of outer to inner

thicknesses. Therefore, it can be expected that the differences between the NAFR and AFR, i.e. between $(V - V)$ and $(V - T)$ and also $(T - T)$ and $(T - V)$, have to remain constant approximately for different ratios of $\dfrac{b}{a}$, as can be observed in Fig. 3.
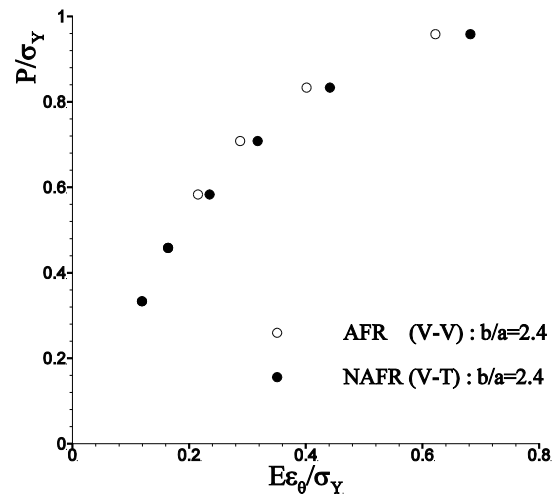
Fig. 4. Comparing $(V - T)$ and $(T - V)$ for circumferential strain of the outer surface with increasing pressure, perfect-plastic.
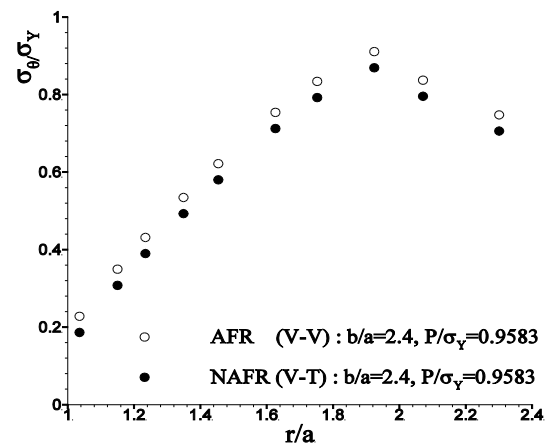
Fig. 5. Comparing $(V - T)$ and $(T - V)$ for circumferential stress distributions, perfect plastic.
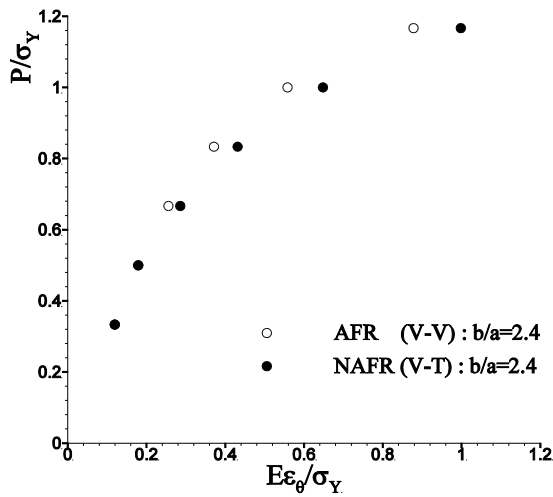
Fig. 6. Comparing $(V-T)$ and $(T-V)$ for circumferential strain of the outer surface with increasing pressure, linear hardening.
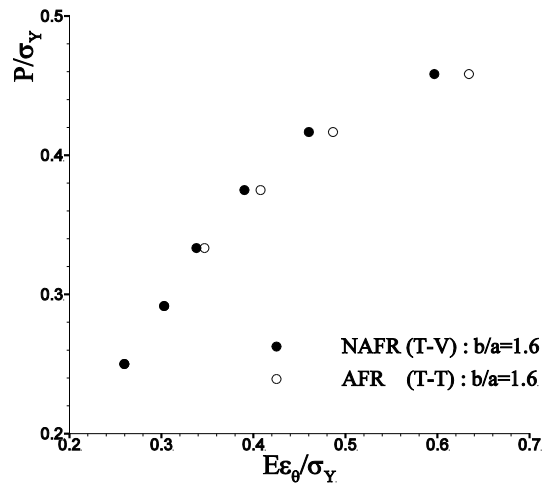
Fig. 8. A Comparing $(V-T)$ and $(T-V)$ for circumferential strain of the outer surface with increasing pressure, perfect plastic.
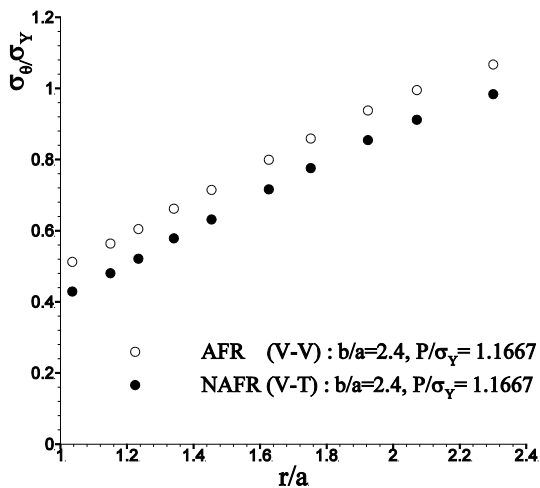
Fig. 7. Comparing $(V-T)$ and $(T-V)$ for circumferential stress distributions, linear hardening.
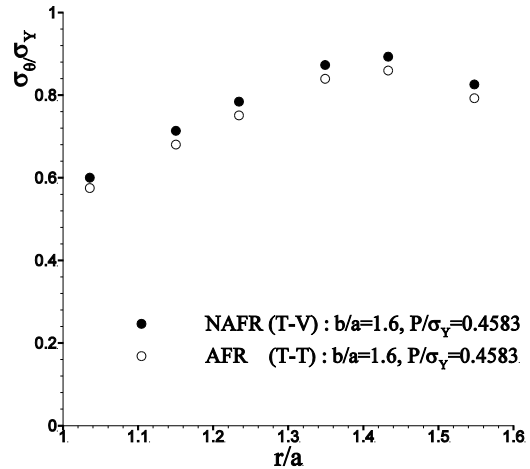
Fig. 9. Comparing $(V-T)$ and $(T-V)$ for circumferential stress distributions, perfect plastic.

To more clarity the ability of the new proposed method, the subsequent studies can be useful. Tresca yield locus can be written as [17]:

$$2\left(J_2'\right)^{\frac{1}{2}}\cos\theta - \sigma_Y = 0, \frac{-\pi}{6} \le \theta \le \frac{\pi}{6} \qquad (21)$$

or,

$$J_2'\cos^2\theta = \frac{\sigma_Y^2}{4} \qquad (22)$$

where J_2' is the second invariant of the deviatoric stress tensor, σ_Y is the yield stress, and θ is the angle of loading in deviatoric plane, which can be shown as:

$$\sin 3\theta = -\frac{3\sqrt{3}}{2}\frac{J_3'}{\left(J_2'\right)^{\frac{3}{2}}} \qquad (23)$$

In the above relation, J_3' is the third invariant of the deviatoric stress tensor. Using trigonometric relations and Eq. (23), it can be stated that:

$$\cos^2 \theta = 1 - \alpha \frac{J_3'^2}{J_2'^3} \qquad (24)$$

where,

$$\alpha = \frac{27}{4} \beta \qquad (25)$$
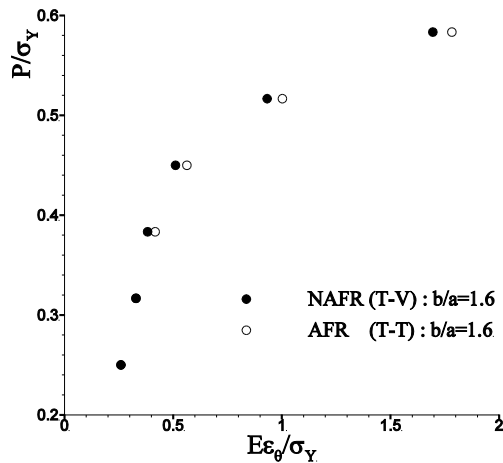
Fig. 10. Comparing $\left(V - T\right)$ and $\left(T - V\right)$ for circumferential strain of the outer surface with increasing pressure, linear hardening.
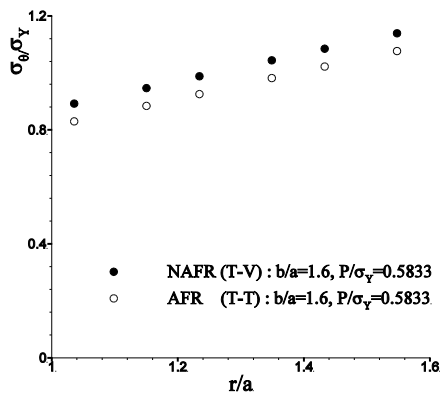
Fig. 11. A comparison between $\left(V - T\right)$ and $\left(T - V\right)$ for circumferential stress distributions, linear hardening.
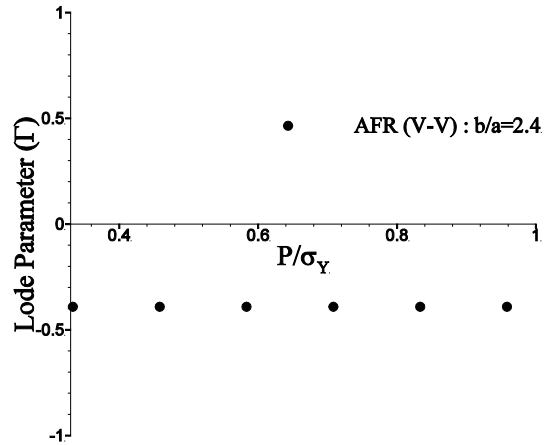
Fig. 12. Variation of Lode parameter in outer surface of the vessel with increasing the internal pressure for perfect-plastic behavior of material and von Mises criterion.

in which,

$$\beta = \frac{\sin^2 \theta}{\sin^2 3\theta} \qquad (26)$$

Finally the Tresca locus can be given as:

$$J_2' \left(1 - \alpha \frac{J_3'^2}{J_2'^3}\right) = \frac{\sigma_Y^2}{4} \qquad (27)$$

Using Eq. (26), the range of α can be determined as:
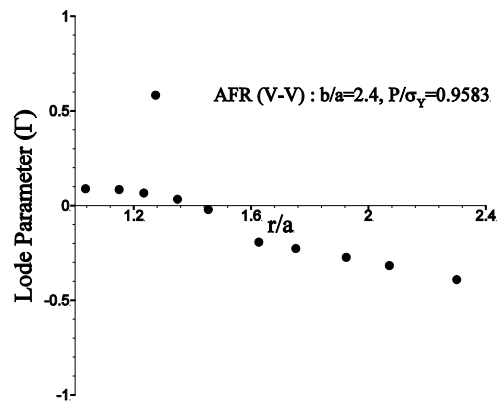
Fig. 13. Variation of Lode parameter with radius for perfect-plastic behavior of material and von Mises criterion.
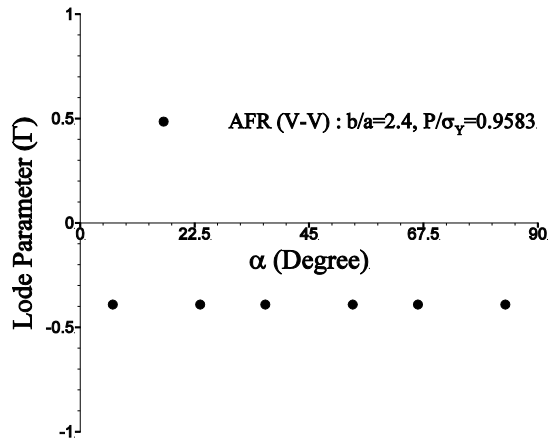
Fig. 14. Variation of Lode parameter versus variation of angle for perfect-plastic behavior of material and von Mises criterion.

$$\frac{3}{4} \le \alpha \le \frac{27}{16} \text{ or } 0.75 \le \alpha \le 1.6875.$$

Some experimental investigations state that the plastic potential locus can be determined as [22]:

$$G\left(J_2', J_3'\right) = J_2'\left(1 - 0.73\frac{J_3'^2}{J_2'^3}\right) \tag{28}$$

which can predict the behavior of materials more precisely than AFR, $\left(V - V\right)$. Comparison of Eq. (27) with Eq. (28) shows that the proposed plastic potential function in Eq. (28) is nearly equal to that of Tresca locus at pure shear. Furthermore, the direction of normal to Tresca locus is constant in the range of $\frac{-\pi}{6} \le \theta \le \frac{\pi}{6}$, hence it may be said that considering $\left(V - T\right)$ can predict the experimental results more accurately than $\left(V - V\right)$ according to [22]. Furthermore, Gao, et al. [10] presented general yield and plastic potential functions as:

$$\begin{cases} F = \left(c_1 J_1^6 + 27J_2'^3 + b_1 J_3'^2\right)^{\frac{1}{6}} \\ G = \left(c_2 J_1^6 + 27J_2'^3 + b_2 J_3'^2\right)^{\frac{1}{6}} \end{cases} \tag{29}$$

where,

$$\begin{cases} c_1 = \left(a_1 + \frac{4}{729}b_1 + 1\right)^{-\frac{1}{6}} \\ c_2 = \left(a_2 + \frac{4}{729}b_2 + 1\right)^{-\frac{1}{6}} \end{cases} \tag{30}$$

By comparing the model with different experimental results, it is concluded that selecting $a_1 = a_2 = 0$, $b_1 = -60.75$, and $b_2 = -25$ can predict the experimental data with good accuracy.

From inserting these values in Eq. (29), it may be deduced that they nearly use $\left(T - V\right)$ in their numerical calculations, which is more accurate than AFR, $\left(T - T\right)$.
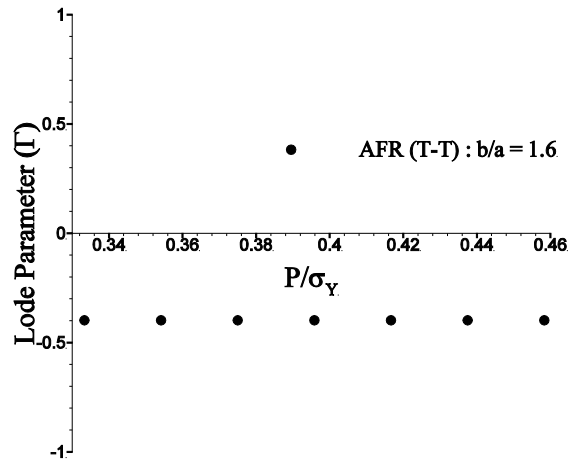
Fig. 15. Variation of Lode parameter in outer surface of the vessel because of increasing the internal pressure for perfect-plastic behavior of material and Tresca criterion.
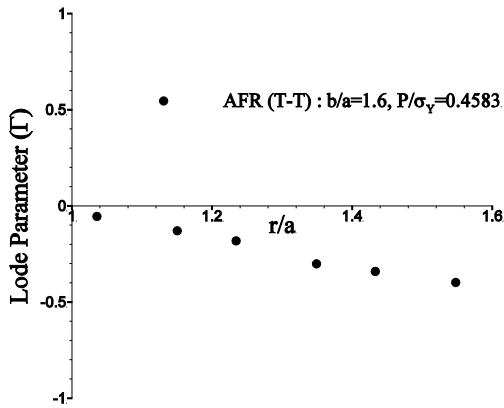
Fig. 16. Variation of Lode parameter versus the variation of radius for perfect-plastic behavior of material and Tresca criterion.
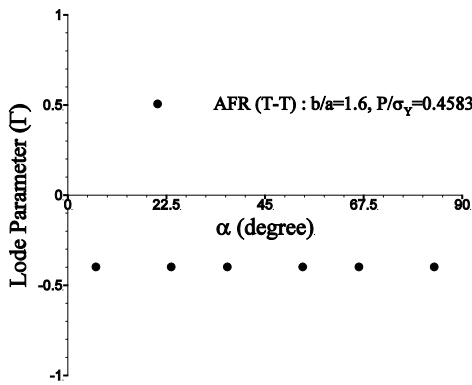
Fig. 17. Variation of Lode parameter versus variation of angle for perfect-plastic behavior of material and Tresca criterion.
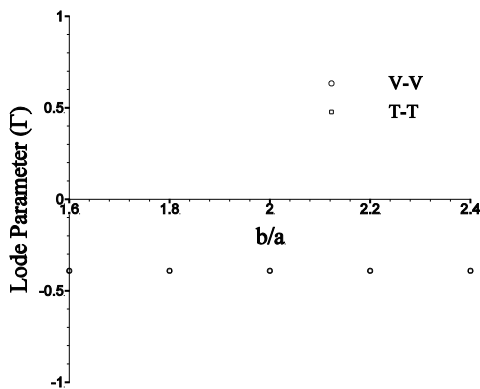
Fig. 18. Variation of Lode parameter with $\frac{b}{a}$.

5. Conclusions

The proposed NAFR was newly implemented with backward Euler method using its consistent elastic-plastic operator in rate-independent plasticity. The results showed that, for an internally elastic-plastic thick-walled cylinder, considering NAFR could help predict the experimental results more accurately than taking the corresponding AFR. Moreover, it was found that the NAFR of $(T-V)$ was better than AFR $(T-T)$ and also NAFR $(V-T)$ was better than AFR $(V-V)$ in terms of predicting the experimental results. In addition to isotropic hardening, the combination of loading (tension-shear) can cause difference between the presented NAFR and corresponding AFR such that, for $\Gamma \to \pm 1$, this difference increased and, for $\Gamma \to 0$, this difference decreased. Finally it can be said that this research confirmed the previous work of the present author on rate-dependent plasticity in steady state conditions [12].

References

[1] T. B. Stoughton and J. W. Yoon, "A pressure-sensitive yield criterion under a non-associated flow rule for sheet metal forming", *International Journal of Plasticity*, Vol. 20, No. (4, 5), pp. 705-731, (2004).

[2] J. Oliver, A. E. Huespe and J. C. Cante, "An implicit/explicit integration scheme to increase computability of non-linear material and contact/friction problems", *Computer Methods in Applied Mechanics and Engineering*, Vol. 197, No. (21-24), pp. 1865-1889, (2008).

[3] T. B. Stoughton and J. W. Yoon, "On the existence of intermediate solutions to the equations of motion under non-associated flow", *International Journal of Plasticity*, Vol. 24, No. 4, pp. 583-613, (2008).

[4] V. Cvitanic, F. Valk and Z. Lozina, "A finite element formulation based on non-associated plasticity for sheet metal forming", *International Journal of*

Plasticity, Vol. 24, No. 4, pp. 646-687, (2008).

[5]   N. Valoroso and L. Rosti, "Consistent derivation of the constitutive algorithm for plane stress isotropic plasticity, part I: Theatrical formulation", *International Journal of Solid and Structures*, Vol. 46, No. 1, pp. 74-91, (2009).

[6]   T. B. Stoughton and J. W. Yoon, "Anisotropic hardening and non-associated flow in proportional loading of sheet metals", *International Journal of Plasticity*, Vol. 25, No. 9, pp. 1777-1817, (2009).

[7]   X. Gao, T. Zhang, M. Hayden and C. Roe, "Effects of the stress state on plasticity and ductile failure of an aluminum 5083 alloy", *International Journal of Plasticity*, Vol. 25, No. 12, pp. 2366-2382, (2009).

[8]   A. Taherizadeh, D. E. Green, A. Ghaei and J. W. Yoon, "A non-associated constitutive model with mixed iso-kinematic hardening for finite element simulation of sheet metal forming", *International Journal of Plasticity*, Vol. 26, No. 2, pp. 288-309, (2010).

[9]   A. Taherizadeh, D. E. Green and J. W. Yoon, "Evaluation of advanced anisotropic models with mixed hardening for general associated and non-associated flow metal plasticity", *International Journal of Plasticity*, Vol. 27, No. 11, pp. 1781-1802, (2011).

[10] X. Gao, T. Zhang, J. Zhou, S. M. Graham, M. Hyden and C. Roe, "On stress-state dependant plasticity modelling: Significance of the hydrostatic stress, the third invariant of stress deviator and the non-associated flow rule", *International Journal of Plasticity*, Vol. 27, No. 2, pp. 217-231, (2011).

[11] F. Moayyedian and M. Kadkhodayan, "A general solution in rate-dependant plasticity", *International Journal of Engineering*, Vol. 26, No. 6, pp. 391-400, (2013).

[12] F. Moayyedian and M. Kadkhodayan, "A study on combination of von Mises and Tresca yield loci in non-associated viscoplasticity", *International Journal of Engineering*, Vol. 27, No. 3, pp. 537-545, (2014).

[13] F. Moayyedian and M. Kadkhodayan, "Implementing the new first and second differentiation of a general yield surface in explicit and implicit rate-independent plasticity", *Journal of Solid Mechanics*, Vol. 3, No. 3, pp. 310-321, (2014).

[14] F. Moayyedian and M. Kadkhodayan, "Combination of modified Yld2000-2d and Yld2000-2d in anisotropic pressure dependent sheet metals", *Latin American Journal of Solids and Structures*, Vol. 12, No. 1, pp. 92-114, (2015).

[15] F. Moyyedian and M. Kadkhodayan, "Modified burzynski criterion with non-associated flow rule for anisotropic asymmetric metals in plane stress problems", *Applied Mathematics and Mechanics*, Vol. 36, No. 3, pp. 303-318, (2015).

[16] A. Ghaei and A. Taherizadeh, "A two-surface hardening plasticity model based on non-associated flow rule for anisotropic metals subjected to cyclic loading", *International Journal of Mechanical Sciences*, Vol. 92, No. 1, pp. 24-34, (2015).

[17] D. R. J. Owen and E. Hinton, *Finite elements in plasticity: theory and practice*, Swansea U. K., pp. 250-340, Pineridge Press Limited, (1980).

[18] E. D. Souza Neto, D. Peric and D. R. J. Owen, *Computational methods for plasticity, theory and applications*, John Wiley and Sons, Ltd., pp. 103-240, (2008).

[19] J. C. Simo and T. J. R. Hughes, *Computational Inelasticity*, Springer-Verlag New York, Inc., pp. 234-305, (1998).

[20] O. C. Zienkiewicz and R. L. Taylor, *The finite element method for solid and structural mechanics*, 6nd ed., U. K., Elsevior Butterworth-Heinemann, pp. 134-205, (2005).

[21] M. A. Crisfield, *Non-linear finite element analysis of solid and structures*, jhon

Wiley, New York, pp. 124-234, (1997).

[22] R. Hill, *The mathematical theory of plasticity*, Oxford University Press, New York, pp. 45-167, (1950).

[23] A. Khan and S. Hung, *Continuum theory of plasticity*, John Wiley & Sons, Canada, pp. 123-208, (1995).

[24] P. V. Marcal, "A note on the elastic-plastic thick cylinder with internal pressure in the open and closed-end condition", *International Journal of Mechanical Sciences*, Vol. 7, No. 12, pp. 841-845, (1965).